Adhesive Bond-line Degradation Detection via a Cross-correlation Electromechanical Impedance-based Approach

Roberto Dugnani, UM-SJTU JI, 800 Dongchuan Rd., Shanghai, 200240 China, roberto.dugnani@sjtu.edu.cn
Yitao Zhuang, Stanford University, Durand Building, Stanford, CA, 94305, zyt@stanford.edu
Fotis Kopsaftopoulos, Stanford University, Durand Building, Stanford, CA, 94305, fkopsaf@stanford.edu
Fu-Kuo Chang, Stanford University, Durand Building, Room 385, Stanford, CA, 94305 fkchang@stanford.edu

This manuscript describes how piezoelectric transducers embedded in the adhesive bond-line of lap-joints can be used to effectively monitor structural integrity. Various lap-joint coupons with embedded piezoelectric transducers were manufactured with and without artificial contamination at the bond-line and tested statically and cyclically. A novel scheme based on the electro-mechanical-impedance (EMI) response of the transducer was implemented to predict the failure of the tested lap-joint samples. The results from the mechanical testing indicated that monitoring the transducer's EMI is an effective way of predicting the failure of the bond-line. Specifically for static tests, local damage to the bond-line was consistently detected at approximately 84% of the failure load for transducers located at the center of the bond-line, whereas for transducers embedded near the edge of the bond-line, the failure of the adhesive was detected at 60% of the failure load. Moreover, preliminary fatigue tests showed that significant changes in the EMI signals were apparent starting at 60% of the life of the bond-line. In addition to the mechanical testing, the effectiveness of the proposed EMI-based scheme was investigated by means of a 3D finite elements model (FEM) corresponding to the specific coupon geometry tested and through a 2D analytical solution.

INTRODUCTION

Adhesively bonded joints are attracting increasing interest particularly in the automotive and aerospace industries due to the relative structural advantages compared to more conventional joining methods such as welding and riveting. Regretfully the assessment of the bonding interface integrity is a very challenging problem and up-to-date the usage of adhesive bonds is for the most part limited to non-structural elements. In addition to the traditional non-destructive inspection (NDI) techniques such acoustic scans, more recently, various Structural Health Monitoring (SHM) techniques have been proposed to monitor *in situ* the presence of damage and/or weak adhesive bond-lines.

Recently, Kouhei et al.[1] developed a SHM system to detect the degradation of the adhesive bond-line on carbon fiber reinforced plastic components bonded to aircraft structures. The SHM system proposed by Kouhei et al.[1] could qualitatively evaluate the structural integrity of the bond-line by analyzing changes in the amplitude and phase of Lamb waves traveling through the bonded components. The diagnostic acoustic waves described in Kouhei et al.[1]'s

work were generated by micro fiber composite piezoelectric actuators embedded in the structure. In the study the acoustic signal traveling in the structure after the structure had been overloaded were recorded and compared to the pristine structure's signature signal. The findings from the proposed SHM technique were also compared with reference data generated by ultrasonic A-Scans. The study showed a good correlation between the proposed SHM method and the ultrasonic A-scans, yet the proposed approach was structure-specific and no explanation was offered on how to extend this type of analysis to structures other than the one considered in the study.

Preisler et al.[2] proposed a strain-based SHM system for single and double bonded lap-joints. The proposed system consisted of monitoring out-of-plane deformations near the edges of the bonded region on the lap-joint. The SHM system could rely on any strain measuring device (e.g., strain gauges, etc.) placed at a location parallel to the edge of the adhesive and at a specific distance shown analytically to be strain-free under normal loading conditions. The proposed monitoring locations were advantageous as they were insensitive to the magnitude of the external loading (for nominal loading conditions) and provided the most sensitive response to bond-line structural changes. The chosen locations were also of high interest due to the higher likelihood of damage initiation at the edges of the adhesive. Validation of the method was offered both through a FE model and by means of various tests on lap-joint coupons. The effects of changes in the adhesive properties due to environmental effects and the potential load path change due to damage at locations other than at the lap-joints were not addressed in the study.

Recently Poveromo et al.[3] discussed a SHM method based on quantitative percussion diagnostics (QPD) to quantify the quality of bond-line in fiber reinforced composite materials. The technique was implemented by impacting the structure of interest using a stainless steel rod containing a force sensor accelerated by an electromagnetic coil to a pre-established impact velocity. The coefficient of restitution of the structure was then computed based on energy conservation principles and its value used to evaluate the local bond-line quality. The research also presented a numerical validation of the concept for the composite structure of interest. Preliminary testing and FEM results indicated that the technology might be able to detect low shear-strength bonds between flat composite laminates. Although yielding promising results, the method could not be easily implemented on large scale. Also the method's sensitivity is likely affected by the lap-joint's materials and construction.

Malinowski et al.[4] investigated the correlation between the adhesive bond strength and features of the EMI signature of piezo-electric transducers bonded to the surface of the adhesively bonded plates. Various plates were tested after applying a known amount of silicone-based release-agent solution on the plates' surfaces before the application of the adhesive. Different amount of release-agent solution at the interface were expected to yield different adhesive cohesion strengths. An index based on the calculation of the Frechet distance between each EMI curve and the corresponding EMI curve for the pristine sample was then computed for each bond-line contamination level. Although differences across samples were detected, the

correlation between the calculated Frechet distance-based index and the degree of contamination were found to be generally weak.

Elsewhere Malinowski et al.[5,6] studied the EMI signature of piezoelectric transducers bonded to plates and resonated thought the thickness. The testing was performed on both weak (i.e., intentionally contaminated bond-lines) and strong bonds. The SHM method considered the effects of the bond-line contamination on both the root-mean square (RMS) of the conductance and the frequency shift of the first resonant mode. Although the experimental results indicated that a separation between weak bonds and strong bonds was possible, nonetheless no attempt was made to model the behavior of the transducers and their interaction with the structure.

Similar to Malinowski et al.[4,5,6], Gulizzi et al.[7] also used EMI-based techniques to monitor the degree of curing of an adhesive bond-line on aluminum lap-joints. The testing conducted by Gulizzi et al.[7] was carried out in a frequency range corresponding to the resonant modes of the aluminum structure analyzed (i.e., 20-80 kHz). The method appeared to be able to capture differences on a large scale as for the case of incomplete curing of the adhesive bond-line. Nonetheless, because of the use of low frequency, the relative wavelength of the acoustic signal was likely too long to accurately capture any localized incipient weakening of the adhesive bond-line.

Although strain reading from optical fibers embedded in bond-lines yielded promising results[8,9], ultrasound-based methods are generally the preferred choice for predicting the fitness-for-service of lap-joint adhesives. The work of Smith and Weise[10], and of Weise et al.[11] presented results from a comprehensive array of experiments aimed at understanding the benefits and limitations of various ultrasound-based NDI methods. Recently Roach et al.[12] also presented a comprehensive study comparing different NDI techniques including thermographic-based inspection and acoustic methods, and discussed the benefits of each technique. Smith and Weise[10] noted that ultrasonic-based techniques either relied on pressure (P) waves or shear-vertical (SV) waves and suggested that SV-waves should be more effective in detecting weak adhesive bond-lines as lap-joint's adhesives normally supported shear loads. The work of Nagy[13] correspondingly supported the notion that SV-waves were more sensitive to variations in the bond-line integrity. Similarly to Smith and Weise[10], Munns et al.[14] conducted a comprehensive survey of NDT methods applied to bonded joints and also concluded that acoustics-based techniques implementing SV-waves were more sensitive to detecting changes in the interfacial properties. Similarly, Clark and Hart[15] showed that normal incidence shear waves were more successful than longitudinal waves in detecting small liquid-filled gaps in layered systems. Cheng and Taheri[16] proposed monitoring lap-joints' bond-line integrity using pitch-catch technique implemented by means of piezoelectric transducers directly attached on the plates' surfaces. An analytical and a series of finite element analyses were carried out to investigate the use of shear waves to monitor the structural integrity of the bond-line. An analogous method was also proposed by Di Scalea et al.[17] who examined the transmission of the lowest-order shear Lamb waves across the overlap of lap–shear joints. Most recently, Zhuang et al.[18] proposed employing a piezoelectric transducer embedded in the lap-joint's bond-line and monitored the

EMI of transducers resonated in the extensional mode. Changes in the electromechanical impedance were then used to successfully diagnose the degradation of the bond-line.

In the next section the fundamental physical principles of some of the most widely used ultrasound-based techniques for adhesive bond characterization are briefly presented. Some of the advantages and limitations of each method are also succinctly addressed.

Normal Incidence Narrow-Band Pulsed Spectrometry

Normal Incidence Narrow-Band Pulsed Spectrometry relies on narrow-band acoustic waves generated by piezoelectric transducers. The technique is implemented either by pulse-echo (i.e., using one transducer to both generate the acoustic signal and record the reflected signal) or pitch-catch by through-transmission mode where an emitter and a receiver are placed on the surface of the structure a few wavelengths apart. Although the method can successfully detect gross defects in the bond-line, it's efficacy in detecting less obvious defects, such as 'kissing bond', is still debated[10,11].

Swept-Frequency Technique

The swept-frequency method determines the resonant frequencies of the probed structure by exciting it with a broad-band, chirp signal. Among the advantages of the method is that it concurrently excites multiple structural resonant modes[19]. Preliminary tests on adhesive bond-lines by Smith and Weise[10] confirmed that the amplitude of the response signals and the resonant frequencies were affected by the mechanical properties of the adhesive and by the quality of the bond-line interface.

Oblique Incidence Ultrasonic technique

The oblique incidence technique is similar to the Normal Incidence Spectrometry method but it consists of exciting both P- and SV-wave (depending on the angle of incidence) rather than P-waves alone. Regretfully, experimental results reported by Weise et al.[11] suggested that 'kissing bonds' could not be consistently detected with this method due to the high sensitivity to the placement of the transducer on the structure and to the signal's incident angle.

Guided waves Ultrasonic technique

Guided waves can be considered a variation of the oblique incidence technique as this method is implemented by placing the emission transducer and the reception transducer few wavelengths apart along the surface of the structure. The advantage of guided-waves is that the acoustic signal is able to scan larger sections of the adhesive as the signal is reflected within the adhesive material several times before reaching the detection probe. Smith et al.[10] and Di Scalea et al.[17] indicated that good detection of weak bonds might be achieved by using guided waves.

EMI BASED DIAGNOSTIC

In this manuscript we expand on the preliminary experimental work of Zhuang et al.[18] and the analytical work of Dugnani and Chang[20], and develop a novel method to interpret the EMI response of a piezoelectric transducer fully embedded in a lap-joint's bond-line and resonated longitudinally. Similarly to other acoustic techniques proven to be effective in detecting bond-line adhesive degradation, the proposed method relies on SV-waves as the principal acoustic signal source as clearly shown by the analytical work of Dugnani and Chang[20]. The main focus of this research is to:

(i) determine what effect the degradation at the adhesive/adherend interface has on the EMI signatures of the embedded transducers, and

(ii) exploit the changes in the EMI signature to predict the bond-line failure.

In the first part of this section we introduce a 3D Finite Element Model (FEM) of the smart lap-joint coupons. The goal of the numerical model is to help describe the behavior of the EMI signal of the embedded transducer as the adhesive/adherend interface was virtually degraded. In the second part of this section, we describe the expected EMI signature of the transducer based on the 2D analytical solution proposed by Dugnani and Chang[20]. In the analytical solution, the adhesive/adherend interface degradation is modeled through the equivalent complex transverse springs of stiffness K_T. A similar approach to model the adhesive/adherend interface degradation has been successfully implemented in the past by various authors[21,22,23,24,25,26,27,28]. Finally, an EMI-based method to detect structural integrity is proposed and subsequently validated by means of extensive static and fatigue tests on various lap-joint coupons.

Numerical Analysis

Commercially available finite element analysis software, ABAQUS 6.12, was used for the FEM simulations. The numerical model included the adhesive layer, and the piezoelectric transducer in a configuration similar to the one used in the experimental testing. The software used a linear parametric solver with over 65,000 degrees of freedom and eight-node brick elements (C3D8E). The mesh had a typical dimension of 100 μm to accurately capture the motion and deformation of the sensor. The transducer's actuation frequency was varied from 50 kHz to 1.2 MHz in 1 kHz incremental steps. Table 1 shows a detailed list of the material properties used in the simulation.

For wavelengths much longer than the thickness of the degraded layer, the introduction of reduced-shear modulus at elements at the interface is analogous to the use of transverse springs of stiffness K_T at the interface boundary, a method successfully used in the literature to model weak interfaces[21,22,23,24,25,26,27,28]. In the numerical study, one side of the bond-line was degraded to simulate a progressive reduction in the carrying load at the adhesive interface (Figure 1, right-hand side). Various simulations were run to model the degradation progression which, in the scenario considered, started at the edges of the adhesive and progressed towards the center of the sample. Although the described failure mode was not directly verified during testing, the tested coupons' failure patterns were consistent with the adhesive's debonding originating at one end of

the adhesive and propagating towards the opposite end. Catastrophic failure generally occurred as the debonded area reached approximately half to two-thirds of the bond area. The pattern propagation considered in this work has been described as 'commonly occurring' by other authors[2]. The degradation of the bond-line was modeled numerically by reducing the shear modulus in the 10μm-thick layer in contact with the metal plates (shear modulus reduction, $G_{b'}=G_b/10$). For the geometry and mechanical properties considered, the degradation introduced at the interface corresponds to a value of the shear spring stiffness $K_T \approx 2 \cdot 10^{13}$ *Pa/m* and the normal spring stiffness $K_N \approx 2.5 \cdot 10^{13}$ *Pa/m*. The value of the shear spring stiffness, K_T, chosen in this study is in the same order of magnitude of the one reported by Rokhlin et al.[24], and Baltazar et al.[28] for lap-joint's adhesives near failure. No value for K_N has been found in the literature but the magnitude of K_N is likely irrelevant when the propagation of SV-waves is considered.

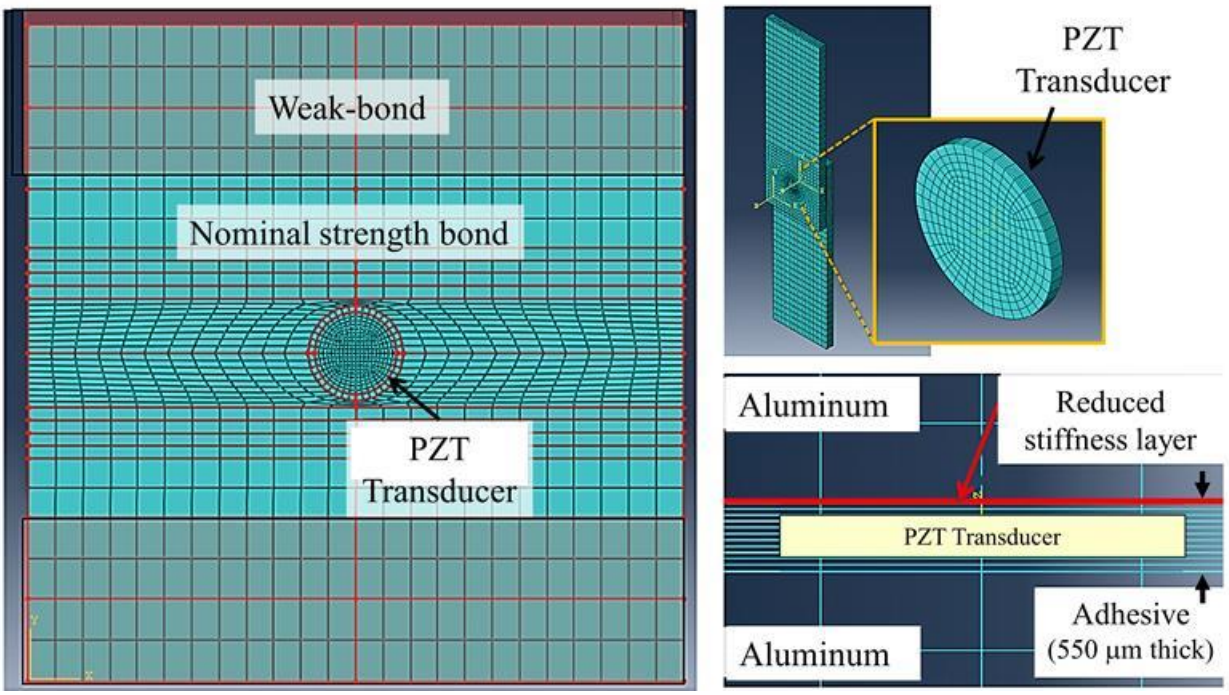

Figure 1. Example of mesh used in the numerical simulation showing the reduction of stiffness of the interfacial elements (right bottom in red), and top view of the bond-line including the nominal strength element and weak bond elements (left).

Figure 1 shows an example of the mesh used in the numerical simulation. Part of the bond-line area (square shape from top view) was degraded to reflect the propagation of the degradation as illustrated in Figure 1 (left). The geometry and dimensions of the coupon considered are shown in details in Figure 2. The adhesive film was sandwiched between two aluminum plates and the piezoelectric transducer was embedded at the center of the adhesive film. The samples' geometry was chosen based on the recommendations outlined by ASTM D 1002-10[29]. The width of the sample was 2.5 *cm* and the approximate bond-area 6.45 cm^2. The piezoelectric transducer had a thickness of 0.2 *mm* and diameter of 3.175 *mm*. The Young modulus and density of the transducer were chosen based on typical reported PZT-5 values. The

adhesive's Young's modulus was chosen based on the (static) value reported by the adhesive's vendor[30] and was found to be consistent with the value measured by Ha et al.[31]. The density of the adhesive, ρ_b, and the Poisson ratio, ν_b, were chosen based on the nominal values reported by the vendor[30]. The loss factor, η_b, was selected as 0.01 based on generic values for epoxy materials as reported in the literature[32].

Table 1 Material properties of the lap-joint components

	Piezoceramic	Adhesive
Material	PZT-5A	Hysol EA 9696
Elastic modulus (E_a, E_b) (GPa)	61	1.9
Mass density (ρ_a, ρ_b) (kg/m^3)	7700	1140
Poisson ratio (ν_b)	–	0.361
Piezoelectric constant (d_{31})(C/N)	$-175\cdot10^{-12}$	–
Permittivity constant (ε_{33})(Farad/m)	$1750\cdot\varepsilon_0$	–
Quality Factor (Q)	80	–
Mechanical loss factor (η_b)	–	0.01

Analytical Analysis

In additional to the numerical simulation, an analytical study based on the work of Dugnani and Chang[20] was implemented to investigate the EMI response of a piezoelectric transducer as damage was introduced at the interface with the metal plates. Dugnani and Chang[20] showed that the behavior of a transducer excited longitudinally is influenced by the degradation of the adhesive/adherend interface. Specifically, for the 2D case considered in the analysis, the electro-mechanical admittance of the transducer, $Y(\omega)$, is expected to behave as:

$$Y(\omega)=i\omega C_0\left\{\left(1-k_{13}^2\right)+k_{13}^2\left[\frac{1}{H(\omega)}+\frac{2\left[U_{S,nf}+U_{S,ff}\right]}{u_a^2K_a\left(1+\eta_a i\right)}\right]^{-1}\right\} \tag{1}$$

where C_0 stands for the transducer's capacitance, $H(\omega)$, for the complex dynamic amplification factor, k_{13}, for the electro-mechanical coupling factor, K_a, for transducer's longitudinal static stiffness, u_a, for the transducer's displacement, and $U_{s,nf}$ and $U_{s,ff}$ for the strain energy of the adhesive film in the near-field (i.e., directly above and below the transducer) and in the far-field respectively. The equations for the adhesive's strain energy for both the far-field and near-field are given by:

$$U_{S,ff}=\sum_i u_i^2W\left[G_b\left(\chi_{ff}-1\right)^2\frac{2\pi}{t_b\gamma_i}+E_{eq}\left(t_b\gamma_i\right)\frac{4}{3}\pi\left(\chi_{ff}^2+\chi_{ff}+1\right)\right] \tag{2}$$

$$U_{S,nf}=\left(\frac{u_a}{Sin\left(\xi_a a\right)}\right)^2W\left[\frac{G_b\left(\chi_{nf}-1\right)^2a}{t_{b0}}\left(1-\frac{Sin\left(2\xi_a a\right)}{2\xi_a a}\right)+\frac{2}{3}E_{eq}\left(\xi_a a\right)\left(\xi_a t_{b0}\right)\left(1+\frac{Sin\left(2\xi_a a\right)}{2\xi_a a}\right)\left(\chi_{nf}^2+\chi_{nf}+1\right)\right]$$

with $$E_{eq} \equiv \frac{\lambda_b^2(1-\nu)+2G_b[G_b+\lambda_b(1-\nu)]}{2G_b(1+\nu)} \quad (3)$$

The terms u_1 and u_2 indicate the amplitude of the SV- and P-wave respectively, γ_1 and γ_2 the bond-line's SV-wavenumber and P-wavenumber, ξ_a, the embedded transducer's wavenumber, W and t_{b0} the width and thickness of the adhesive film, a, the transducer's half-length, and χ the sliding ratio, a parameter related to the transverse spring constant, K_T, though the relationship:

$$K_T = \frac{G_b}{t_{b0}} \frac{(1-\chi)}{\chi} \quad (4)$$

Clearly, based on Dugnani and Chang's model[20], the strain energy in the adhesive -and hence the EMI response of the transducer- is influenced by the adhesion between the adhesive and the adherend (i.e., the transverse spring stiffness, K_T). Hence, by using the analytical model described by equation 1, it is possible to establish qualitatively the effect on the transducer's EMI response induced by changes in the transverse spring stiffness both in the transducer's far-field and near-field. More details on the derivation of equations 1 through 4 can be found in Dugnani and Chang[20].

MECHANICAL TESTING

Both static and fatigue tests were carried out on lap-joint specimens with embedded piezoelectric transducers. The manufacturing of the test coupons was based on the recommendations outlined by ASTM D 1002-10[29]. Various coupons were prepared and tested but only twelve coupons were found to have a consistent adhesive's thickness and hence only those were considered in the analysis. An approximately 0.5 *mm* thick adhesive film (Hysol EA 9696) was sandwiched between two 2024 aluminum strips, 3.1 *mm* thick, and 2.5 *cm* wide. For each specimen, a piezoelectric transducer by APC 850[33] 0.2 *mm* thick, and 1.9 *mm* in diameter was embedded at the center of the bond-line. In a single instance, multiple transducers were embedded in the specimen's bond-line. The length of the bonded region, L_b, was approximately 2.5 *cm* for the single embedded transducer specimens, while L_b= 5.1 *cm* was used for the specimen with multiple transducers embedded. Figure 2 shows a schematic drawing of the test coupon used for the both the static and fatigue shear strength tests including the relevant dimensions. Also Figure 2 (right-hand side) shows a photograph of the experimental test setup. A commercially available impedance analyzer manufactured by Sine-phase (model 16777k)[34] was used to collect the electrical admittance of the transducers during the mechanical tests. The amplitude of the excitation signal was held constant at 0.2*V* in all cases.

Prior to the application of the adhesive films, the aluminum plates were prepared by abrading the bonding surface using 100-grit sandpaper followed by rinsing in DI water, acetone, and isopropanol alcohol. For various samples, one surface of the aluminum plates was intentionally contaminated with graphite powder to introduce a weaker interface between the adhesive and the adherend. Figure 2 shows an exploded view of the test coupon assembly including the graphite contamination at the bond-line. After assembling, the samples were cured

in a convection oven first by increasing the temperature from 20°C to 121°C in one hour and subsequently by holding the temperature at 121°C for two hours before gradually cooling. During the curing cycle, the samples were vacuum bagged to maintain a uniform pressure between the adhesive film and the plates. The thickness of the adhesive film after curing was measured as $500\pm100\mu m$. Those samples which did not display a uniform film were discarded and not considered in the analysis. Although not directly verified, the curing cycle was expected not to affect the response of the piezoelectric transducer as the peak curing temperature was only 30% of the Curie temperature (365°C) for the used piezoelectric material[33].

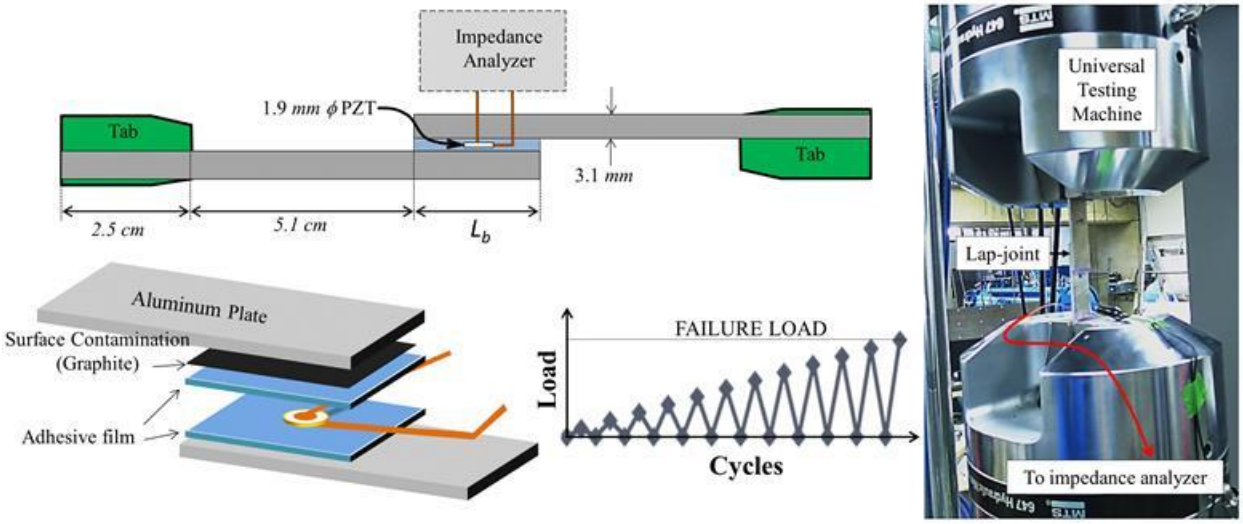

Figure 2. Schematic representation of the lap-joint test coupon with embedded 1.9*mm* diameter disk PZT (left), and the experimental test setup (right).

Static and fatigue tests were carried out using a MTS-model 370 load frame with a rated capacity of 250 *kN*. For the static tests, the samples were loaded and unloaded at a constant rate of 1 *kN/sec* up to a pre-determined peak load and held at such load for five seconds. At the end of each loading cycle, the samples were unloaded and the electrical admittance of the transducer was recorded using the impedance analyzer. The peak load applied to the specimen was incremented at each loading cycle until catastrophic failure of the bond-line occurred. A schematic representation of the loading sequence is shown in Figure 2.

The fatigue tests were carried out following the guidelines outlined in ASTM D3136-99 [35]. The sample was loaded by applying a sinusoidal unidirectional axial load with load ratio, R = 0.2. The peak average stress on the adhesive had a magnitude 1.7 *MPa*, the minimum magnitude 0.34 *MPa*, and the testing frequency was set at 3*Hz*. The test was paused every 500 cycles and the electrical admittance for the sample was collected while keeping the specimen unloaded.

DATA ANALYSIS

The electrical admittance of the transducer is a complex measurement expressed in the form $Y(\omega) = G(\omega) + i \cdot B(\omega)$, where $B(\omega)$ is called the susceptance, and $G(\omega)$ the conductance.

Since the structural damping affects mostly the conductance, $G(\omega)$, the latter term is normally used to track structural changes in the system[21,36,37,38]. In addition to the electrical admittance, in this work the resonant frequency, f_R, was also tracked to provide an alternative method to investigate the degradation of the adhesive's bond-line. Although the resonant frequency, f_R, is expected to be less sensitive to the degradation of the bond-line, nonetheless its value is expected to be relatively unaffected by environmental changes and hence also of interest[20].

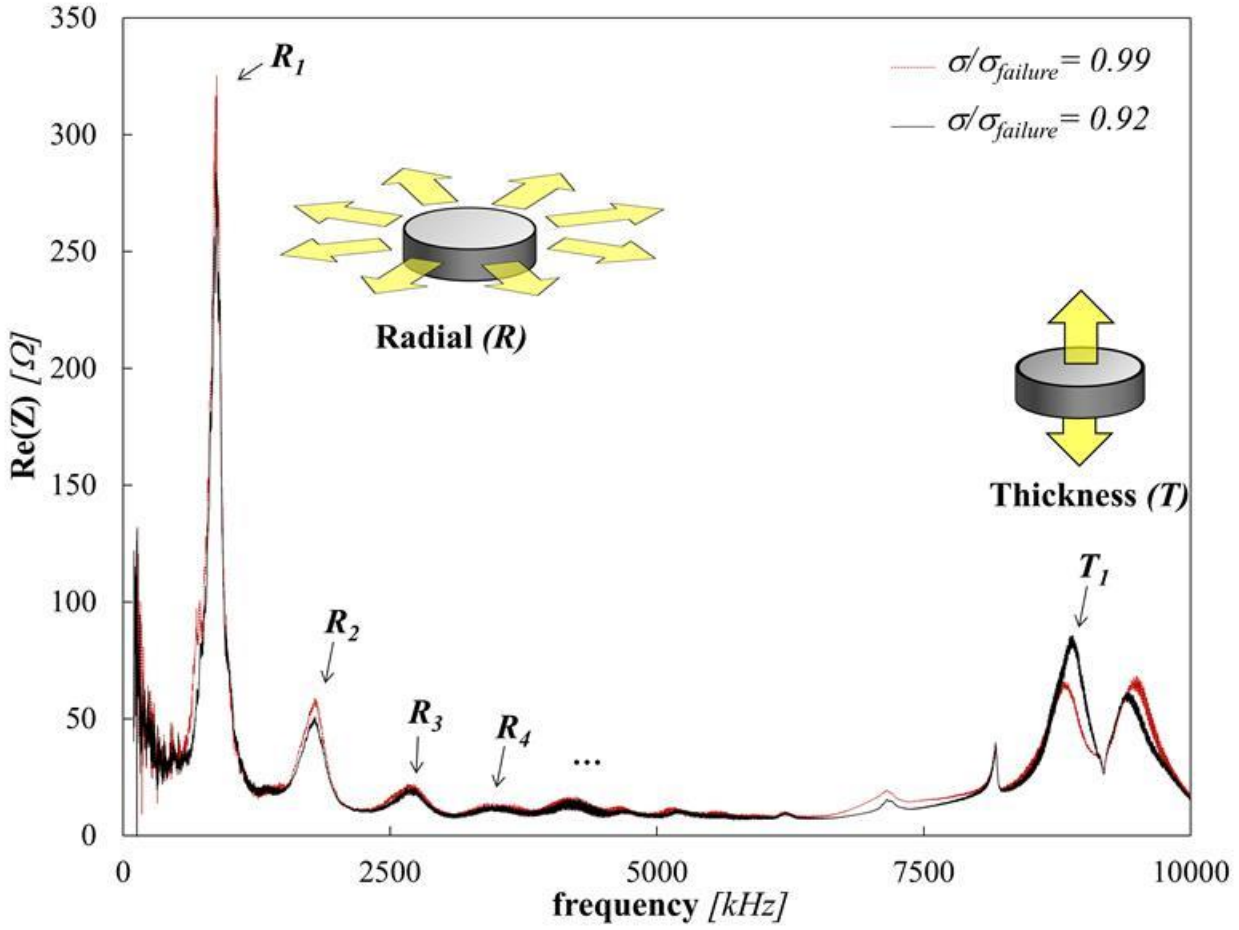

Figure 3. Real part of the electrical impedance signal, *Re(Z)*, versus excitation frequency for a transducer embedded in the adhesive film. The traces corresponded to the signals of the unloaded specimen after the sample was tested at stress levels, $\sigma/\sigma_{failure} = 0.99$ and $\sigma/\sigma_{failure} = 0.92$ (Sample 'B4N1'; the sample dimensions are provided in Figure 2).

Figure 3 shows an example of the real part of the electrical impedance, *Re(Z)*, for an embedded piezoelectric transducer after the sample was loaded to shear stress levels $\sigma/\sigma_{failure} = 0.92$ and $\sigma/\sigma_{failure} = 0.99$, where σ is the peak load for the cycle considered, and $\sigma_{failure}$ is the average stress at failure. In the plot the peaks corresponding to the first (R_1), second (R_2), third (R_3) etc. radial resonant modes, as well as the first thickness mode (T_1) are highlighted. For the transducer's geometry considered, the first extensional resonant mode is distinguishable at about 800 *kHz* while the first thickness resonant mode occurs at approximately 8.9 *MHz*. As shown in Figure 3,

as the bond-line shear stress approaches the failure stress, both the frequency of the resonant peaks and the magnitude of the EMI response vary. In this section we show how changes in the peak frequency and the peak magnitude can be accurately tracked using advance mathematical analytical tools, and how these parameters could be used to effectively assess the degradation of the adhesive film.

EMI Signal Analysis

In the proposed scheme, the cross-correlation of EMI signals is used to precisely track relative changes in the frequency and magnitude of the peak conductance. Specifically, in the scheme, the conductance after the n^{th} cycle, $G_n(\omega)$, is cross-correlated with a reference value, $G_0(\omega)$ and the resulting signal analyzed. A cross-correlation function, $A_n(\omega)$, can then be defined mathematically as:

$$A_n(\omega) = \int_{-\infty}^{+\infty} G_0(\omega)^* G_n(\omega + 2\pi \cdot \tau) d\omega \tag{5}$$

The term τ in Equation 5 stands for the 'frequency lag'.

Figure 4 shows two cross-correlation traces versus the frequency lag, τ, obtained from a semi-static test on a smart lap-joint. The first trace is obtained by cross-correlating the transducer's conductance 'as-manufactured', $G_0(\omega)$, with the transducer's conductance after 14 load cycles, $G_{14}(\omega)$; the second trace in Figure 4 is obtained by the auto-correlation of the reference, 'as-manufactured' conductance, $G_0(\omega)$. Both a distinct shift in the peak frequency, Δf_R, and a change the normalized signal magnitude, $A_{14}(\omega)/A_0(0)$ are clearly observed as a result of the cyclic loading. The peak near $\tau = 0$ in Figure 4 corresponds to the first radial resonant mode (R_1) while the second tallest peak at $\tau = \pm 0.8$ *MHz* corresponds to relative changes between the first radial (R_1) and the second radial resonant mode (R_2). In the analysis performed in this work, only the first resonant peak is considered.

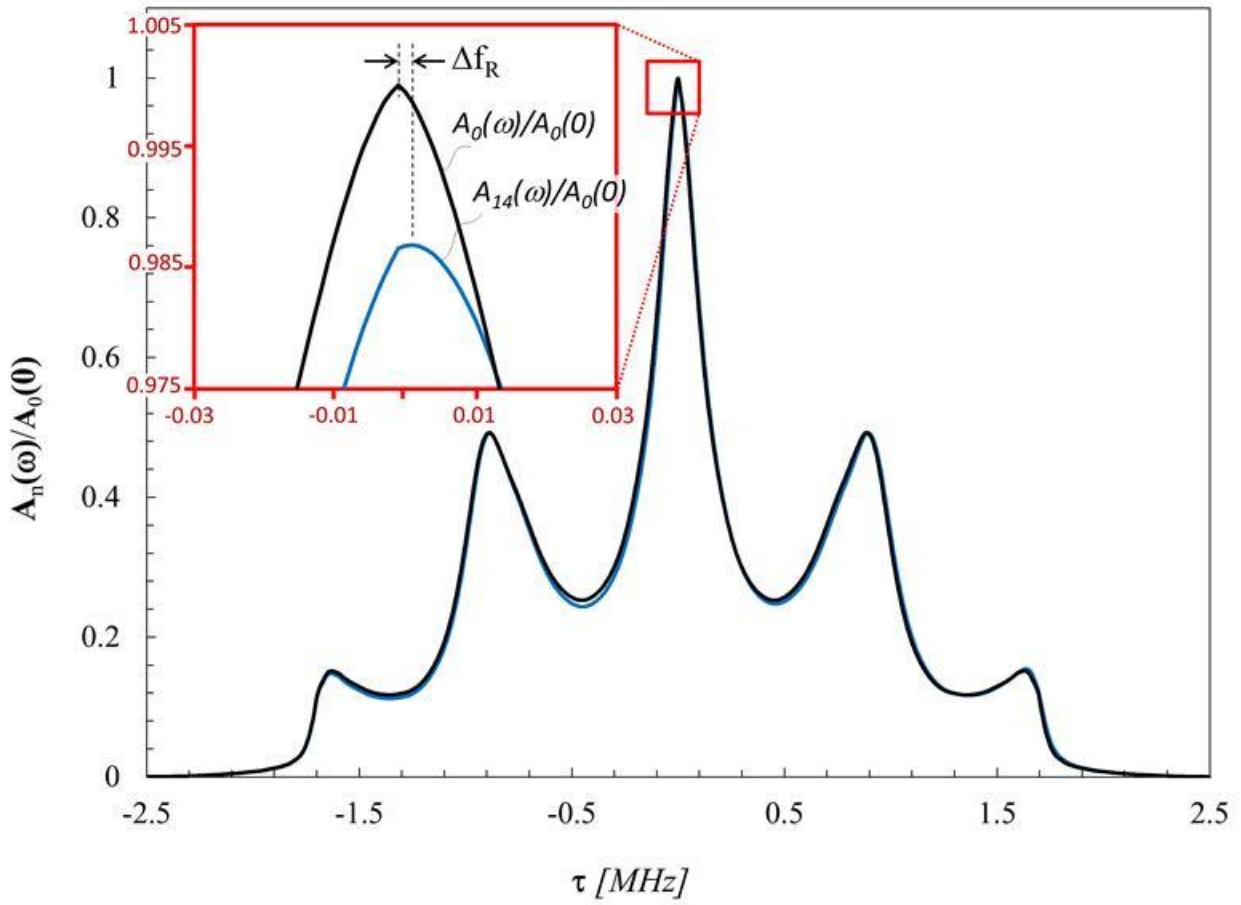

Figure 4. Example of normalized cross-correlation signal, $A_{14}(\omega)/A_0(0)$, for sample 'B8K1' (average stress, σ=2.3 *MPa*).

EXPERIMENTAL AND NUMERICAL RESULTS

Numerical Model

FEM simulations were carried out for various bond-line conditions to study the behavior of the parameters of interest $A_n(\omega)/A_0(0)$ and $\Delta f_R/f_R$ as artificial weakening was introduced along one side of the interface between the adhesive and the adherend. In the scenario considered the degradation at the interface between the adherend and the adhesive initiated at the edges of the adhesive and propagated towards the center of the bond-line. The adhesive damage propagation scenario considered is expected to be of relevance for most lap-joint loaded in shear and failing at the adherend/adhesive interface. In fact the ends of the adhesive have been known to display the highest out-of-plane stress[31] and failures have been reported in the literature to often initiate at these locations. A pictorial representation of the adhesive degradation is presented in Figure 5 on the right-hand side where the weakened area is shown to progressively extend from 50% coverage to 100% coverage.

Figure 5 on the left-hand side shows both the normalized peak cross-correlation, $A_n(\omega)/A_0(0)$, and the normalized change in the peak frequency, $\Delta f_R/f_R$, as calculated based on the

FEM solutions versus the bond-line's percentage area degraded. Interestingly, the computed change in peak frequency $\Delta f_R/f_R$ displays a local minimum as the damaged area reached approximately 76% of the total bond area, while the normalized peak cross-correlation parameter, $A_n(\omega)/A_0(0)$, shows a local minimum as the damage covers about 99% of the load-carrying area.

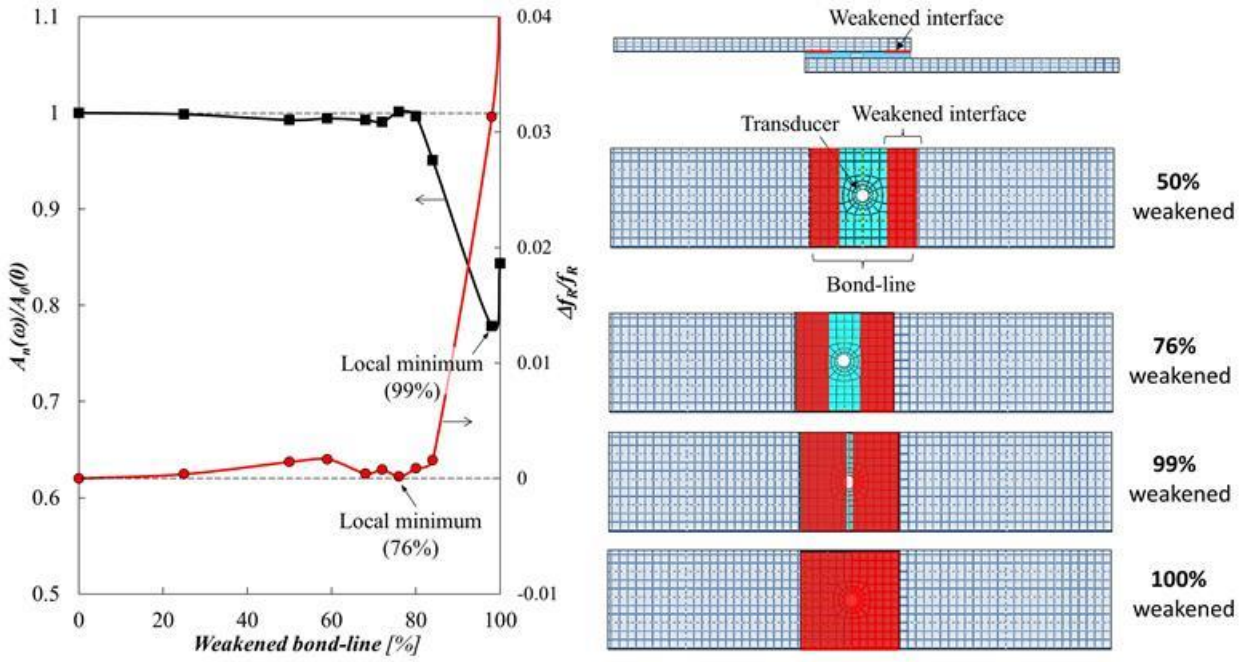

Figure 5. Normalized peak cross-correlation, $A_n(\omega)/A_0(0)$, versus weakened bond-line area coverage (black line, square markers) and normalized change in peak frequency, $\Delta f_R/f_R$, versus weakened bond-line area coverage (red line, circular markers) based on FEM simulations.

Although $A_n(\omega)/A_0(0)$ clearly displays a larger relative variation compared to the resonant frequency shift, $\Delta f/f_R$, for the case considered the latter displays a local minimum prior to the degradation reaching the transducer's near-field. The existence of a local minimum for both the parameter $\Delta f/f_R$ and $A_n(\omega)/A_0(0)$ is of critical importance for this study as the location of the local minima rather than changes in the relative magnitude are used to predict failure. Life estimations based on the detection of a local minimum for either of the parameter described is expected to be more reliable than estimations based on "thresholds" as for instance in Zhang et al.[18], as large variations in the magnitude of the EMI response were observed across different transducers.

Analytical model

The analytical solution described in this section considers a scenario similar to the one addressed in the numerical section. Under this scenario, the degradation at the adhesive/adherend interface initiates at the adhesive edges and subsequently propagates towards the center of the bond-line. This failure scenario has been reported as relatively common on bonded lap-joint structures[2]. Unlike the case described by the numerical model, in the analytical solution derived

by Dugnani and Chang[20] the damage at the interface is introduced symmetrical on both adhesive/adherend interfaces, hence in the analytical model the damage initiates at both edges and on both interfaces simultaneously. The behavior is approximated by initially letting the magnitude of the far-field transverse spring stiffness decrease progressively from an initial value $K_T = \infty$ (perfect bond) to a final value $K_T = 0.3 \cdot 10^{13}$ *Pa/m* while maintaining the near-field spring stiffness infinite. This step represents the damage initiating in the far-field and progressing towards the center of the bond-line. In the second step of the model, the far-field transverse spring stiffness is held constant at $K_T = 0.3 \cdot 10^{13}$ *Pa/m* while the magnitude of the near-field shear spring stiffness is decreased from an initial value $K_T = \infty$ (perfect bond) to its final value $K_T = 0.3 \cdot 10^{13}$ *Pa/m*. This second stage represents the damage reaching the center of the transducer. The results of this simulation are shown in Figure 6. In the left-hand portion of Figure 6's horizontal axis, the spring constant in the far-field is varied (non-linearly) in the range [∞, $0.3 \cdot 10^{13}$ *Pa/m*] whereas K_T in the near-field is held constant (i.e., $K_T = \infty$). In the right-hand portion of Figure 6's horizontal axis, the spring constant in the near-field is varied in the range [∞, $0.3 \cdot 10^{13}$ *Pa/m*] whereas K_T in the far-field is held constant (i.e., $K_T = 0.3 \cdot 10^{13}$ *Pa/m*).

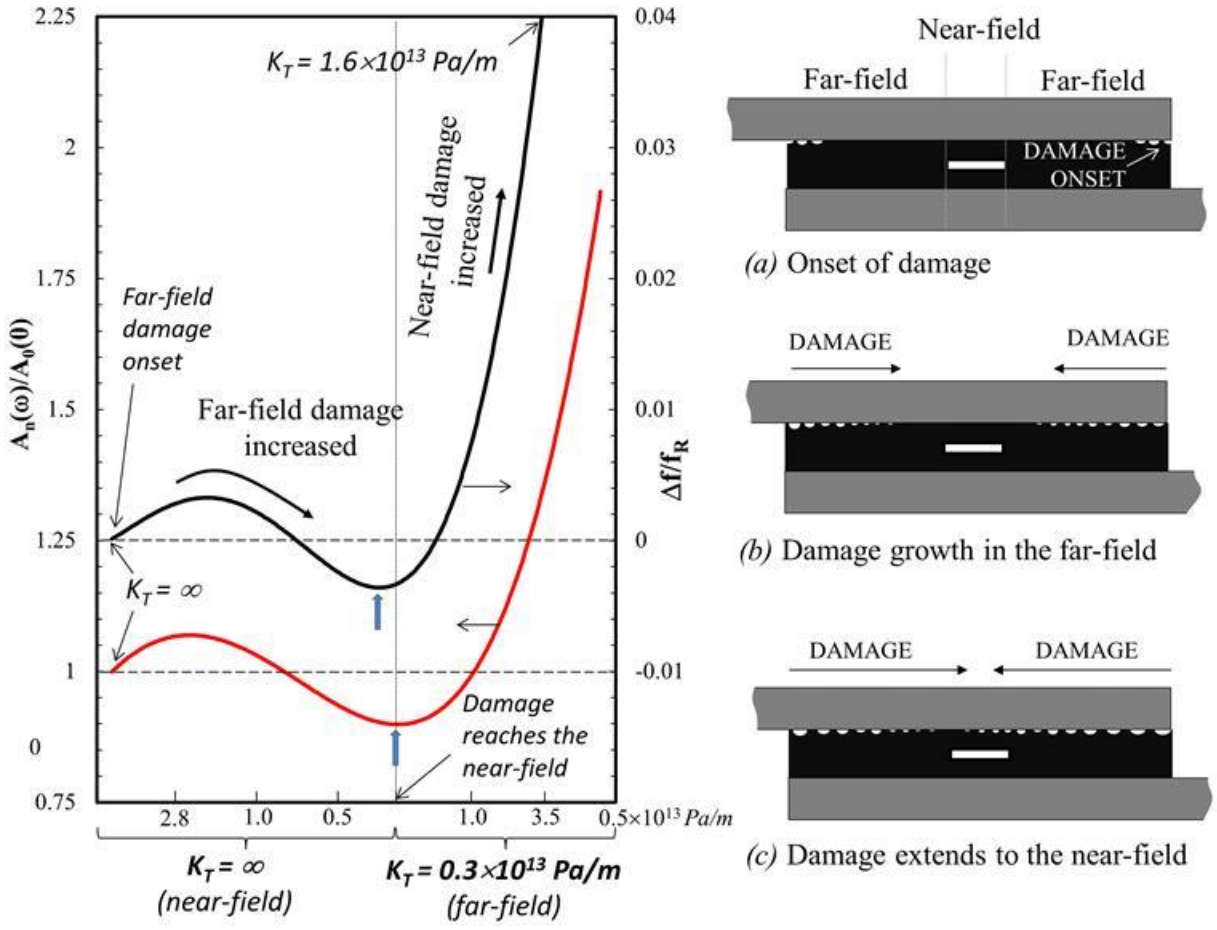

Figure 6. Expected trends for relative change in peak frequency, $\Delta f/f_R$,(black line) and $A(\omega)/A_0(0)$ (red line) as the damage onsets in the far-field (a), progressing towards the near-field (b), and reaching the transducer's

near-field (c). Analytical solution for $2a$=3.175mm,$2t_a$=0.2 mm, $2t_b$=$0.55mm$, G_b=1.9 GPa, ν =0.361, η_b=0.01.

Based on the analytical model and the damage scenario considered, as the interface damage approaches the near-field, the peak frequency $\Delta f/f_R$ decreases steeply followed shortly afterward by the conductance. Although the relative magnitude of $A_n(\omega)/A_0(0)$ displays a larger variation compared to $\Delta f/f_R$, the latter displays a local minimum prior to the degradation reaching the transducer's near-field (Figure 6). This behavior is consistent with the results obtained by the FEM model which were described in the previous section.

Static loading

Various lap-joint coupons both with standard bond-lines and with bond-lines intentionally contaminated by graphite powder were tested semi-statically. Cyclic loads with incrementally higher peak loads were applied to the samples and the transducer's EMI signatures collected after each cycle. Both the peak frequency for the 1st extensional resonant frequency, f_R, and the corresponding cross-correlation peak amplitude, A_n, were computed using the methodology outlined in the previous sections.

Figure 7 shows $A_n(\omega)/A_0(0)$ and $\Delta f_R/f_R$ versus the normalized peak stress at each cycle, $\sigma/\sigma_{failure}$, for three representative lap-joint samples with transducers embedded at the center of the bond-line. Although additional samples were tested results are not shown in the same plot as the impedance magnitude displayed large variations across the samples and only selected results with similar impedance magnitudes were plotted. The samples shown in Figure 7 failed at loads corresponding to an average shear stress of 7.6 MPa, 4.8 MPa, and 6.7 MPa respectively. Although the samples were not artificially contaminated, all failures occurred at the interface between the adhesive and the metal plates. Both $A_n(\omega)/A_0(0)$ and $\Delta f_R/f_R$ are found to be marginally affected at relatively low loads but as the load on the lap-joint approaches structural failure, significant changes in the parameters are evident. The analytical model (Figure 6) and the tests results (Figure 7) might appear to have inconsistent trends in terms of relative change in peak frequency and amplitude, $A_n(\omega)/A_0(0)$. Nonetheless, the carful reader will appreciate that the relative change in peak frequency, $\Delta f_R/f_R$, clearly follows a pattern similar to the one described in the analytical and the FEM models: $\Delta f_R/f_R$ initially keeps relatively stable, gradually decreases to a local minimum, and finally increases drastically as the damaged area reached the transducer. The differences between the analytical model and the experimental results can be attributed to the fact that the horizontal scale for the analytical model (Figure 6) and the experimental data (Figure 7) are not progressing at the same rate as the bond-line damage in the experimental tests is likely to propagate at an exponential rate rather than at a linear rate. Conversely, the trend for the normalized cross-correlation peak amplitude, $A_n(\omega)/A_0(0)$, from testing was not always found to be consistent with the results in the FEM model as a local minimum was not always observable in the test results. Some possible reasons for this apparent

discrepancy between the FEM and the analytical solution are offered later in the discussion section of this manuscript.

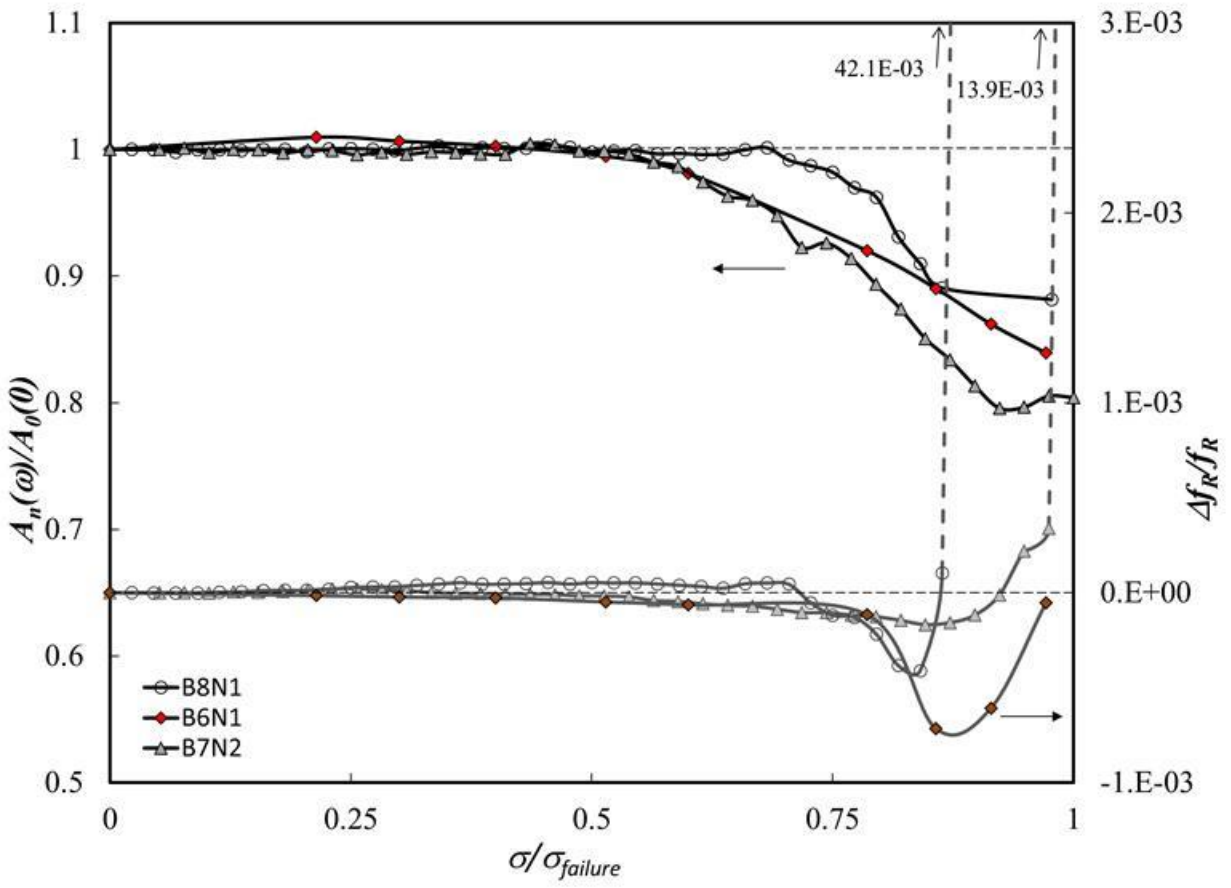

Figure 7. Normalized peak cross-correlation, $A_n(\omega)/A_0(\omega)$, versus normalized peak-stress, $\sigma/\sigma_{failure}$, (black lines, top 3 lines) and normalized change in peak frequency, $\Delta f_R/f_R$, versus normalized peak stress $\sigma/\sigma_{failure}$, (gray lines, bottom 3 lines) from static testing of three lap-shear coupons (per ASTM D 1002[29]).

A total of nine samples with normal bond-lines and three with contaminated bond-lines were statically tested to failure. From the analysis of all data, it is found that a significant changes in the magnitude of normalized peak cross-correlation, $A_n(\omega)/A_0(0)$, occurs in the range $\sigma/\sigma_{failure}$= 0.6-0.7. Although $A_n(\omega)/A_0(0)$ decreases significantly at $\sigma/\sigma_{failure}$> 0.6, only in some instances it reaches a local minimum before failure. Conversely, the parameter $\Delta f_R/f_R$ always shows local minima prior to failure and its behavior is consistent with the trend described by both the FEM model and the analytical solution. This is clear for instance in Figure 7 where $\Delta f_R/f_R$ for the three representative samples analyzed reaches a local minim in the range $\sigma/\sigma_{failure}$ = 0.8-0.9.

Figure 8 shows a plot of the average stress at failure, $\sigma_{failure}$, versus the stress corresponding to the recorded local minimum for the parameter $\Delta f_R/f_R$. The circular makers are used to indicate the results from eleven samples with 2.5 cm × 2.5 cm bond-line, and for one

sample with 2.5 *cm* × 5.1 *cm* long bond-line with a single piezoelectric transducer at the center of the bond-line. The dark markers represents the samples with the artificially weakened bond-line (i.e., contaminated by graphite) while the light green makers shows the results for the standard bond-lines. A linear fit of slope 0.84 fits all the data extremely reasonably which indicates that the minimum value of $\Delta f_R/f_R$ consistently occurs at $\sigma/\sigma_{failure} \cong 0.84$.

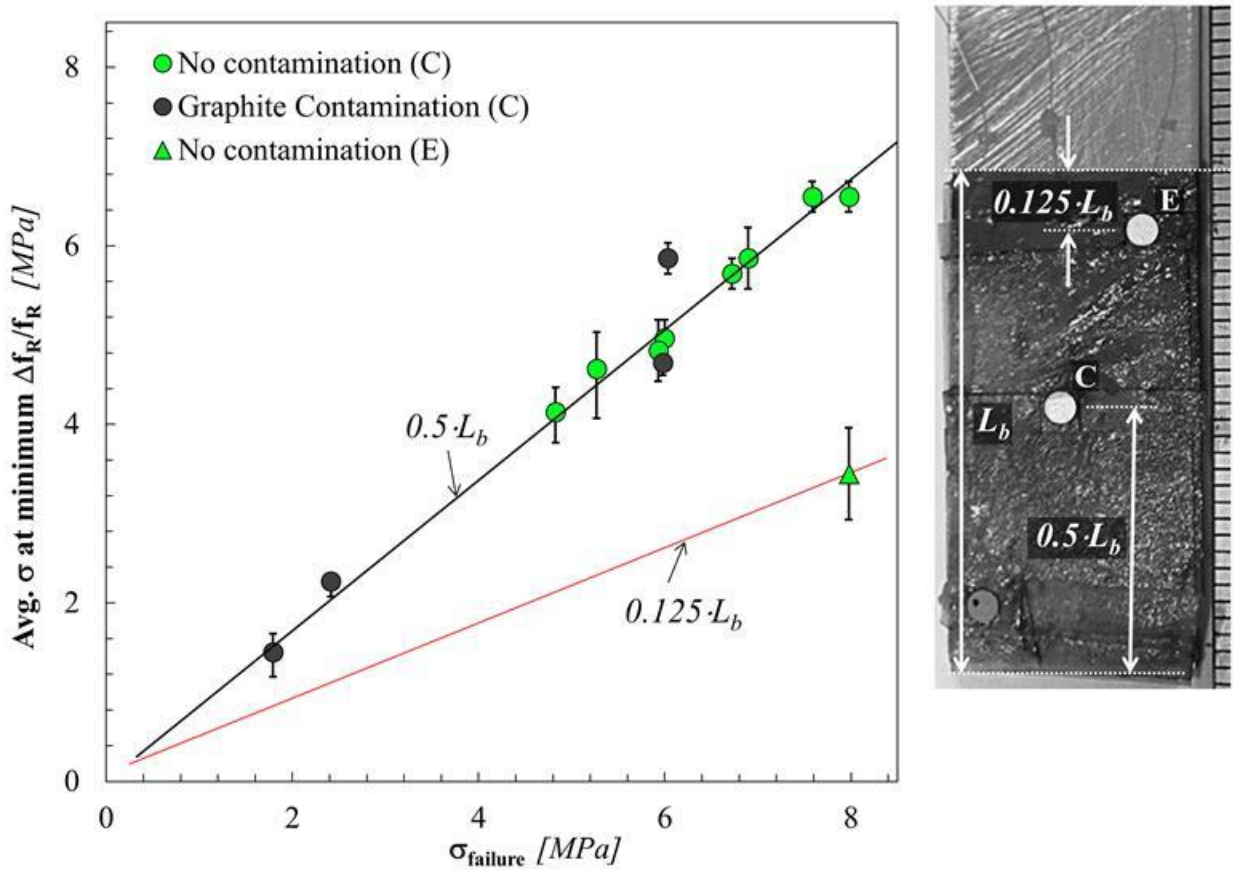

Figure 8. Average stress level when $\Delta f_R/f_R$ reaches a minimum versus the average stress at failure, $\sigma_{failure}$, (circular markers for transducer located at location 'C', at the center of the bond-line; triangular marker for the transducer located at location 'E', near the edge of the bond-line).

Figure 8 also shows the results obtained from the testing of one sample with a 2.5 *cm* × 5.1 *cm* long bond-line but with two transducers embedded in the adhesive. The first transducer was placed at the center of the 2.5 *cm* × 5.1 *cm* long bond-line and the second was located near the edge of the bond-line. The two transducers (marked 'C' and 'E') are shown in Figure 8 on the right-hand side. Although only one sample was tested for this configuration, it is found that the minimum value of $\Delta f_R/f_R$ occurred at $\sigma/\sigma_{failure} \cong 0.6$.

Figure 9 shows more in details the results from the static load test for each of the two transducers embedded in a single bond-line. Transducer 'C' at the center behaved in manner similar to the single transducers tested on the 2.5 *cm* × 2.5 *cm* long bond-line, with a distinct local minimum for $\Delta f_R/f_R$ occurring at about $\sigma/\sigma_{failure} \cong 0.9$. The transducer near the edge at

location ‘E’ on the other hand displays a local minimum for $\Delta f_R/f_R$ at $\sigma/\sigma_{failure} \cong 0.56$. Figure 9 on the right-hand side shows the normalized magnitude of the cross-correlation signal, $A_n(\omega)/A_0(0)$, for the first radial resonant mode versus the peak stress normalized to the average stress at failure, $\sigma/\sigma_{failure}$. The magnitude of $A_n(\omega)/A_0(0)$ decreases slowly as the loading increases but the magnitude sharply increases as $\sigma/\sigma_{failure} \cong 0.9$ for transducer ‘C’, and as $\sigma/\sigma_{failure} \cong 0.56$ for the transducer ‘E’.

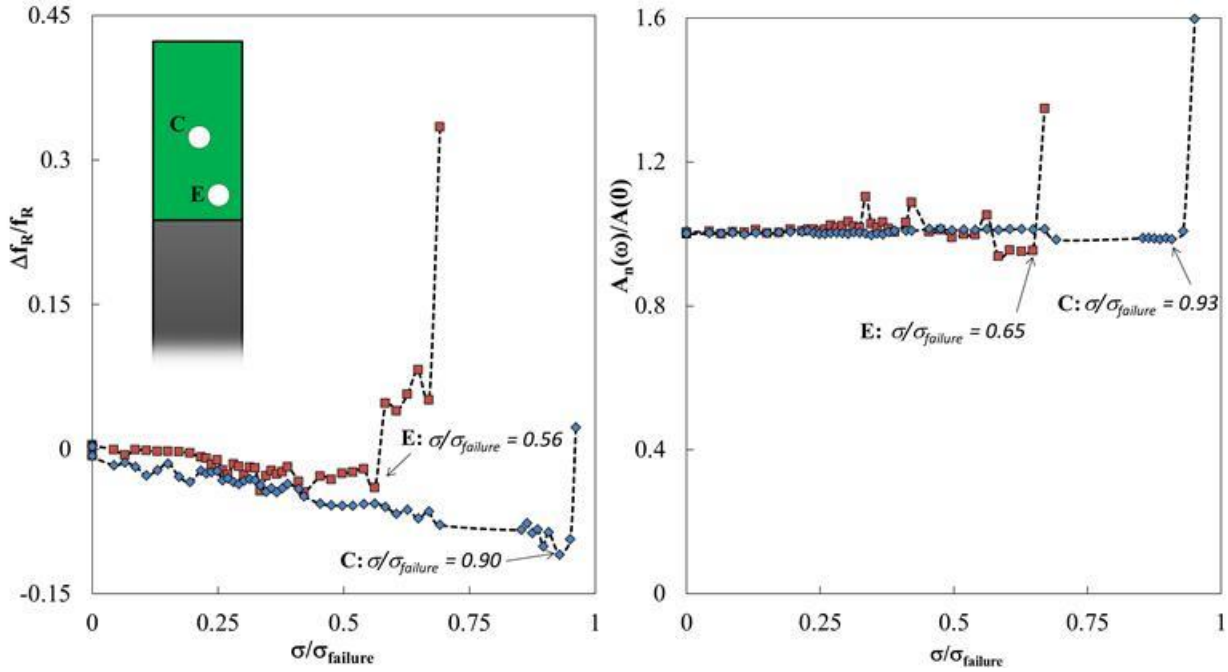

Figure 9. Normalized change in peak frequency, $\Delta f_R/f_R$, versus normalized peak stress $\sigma/\sigma_{failure}$, and normalized peak cross-correlation, $A_n(\omega)/A_0(0)$, versus normalized peak-stress, $\sigma/\sigma_{failure}$, for static testing of three lap-shear coupons (transducer ‘C’ located at the center of the bond-line, diamond markers; transducer ‘E’ located at a distance $L_b/8$ from the edge, square markers).

Thickness and Radial Response

Although the impedance on most lap-joint samples was collected at excitation frequencies corresponding to the 1st radial mode, in a few cases the response of the transducer in the thickness mode (T_1) was considered. Figure 10 shows the EMI-based parameters $A_n(\omega)/A_0(0)$ and $\Delta f_T/f_T$ as computed based on the signals obtained for the transducer’s first thickness resonant mode, T_1. The behavior of both parameters appears similar to the one obtained for the radial mode, with a relatively stable behavior at low loads and large deviations from the initial value near the sample failure. Nonetheless, some important differences between these results and the ones obtained for the first radial mode should be highlighted: first, the magnitude changes are more significant for the thickness mode than for the radial mode; in particular the parameter $A_n(\omega)/A_0(0)$ displays magnitude variations approximately five times larger than the ones observed for the radial mode. Second, the parameter $\Delta f_T/f_T$ decreases steadily and does not reach a clear local minimum near failure as for the case of the radial resonant mode (Figure 10). This

second observation is critical as the type of analysis described in the previous section and carried out for the radial mode is only possible when a local minimum is observed.

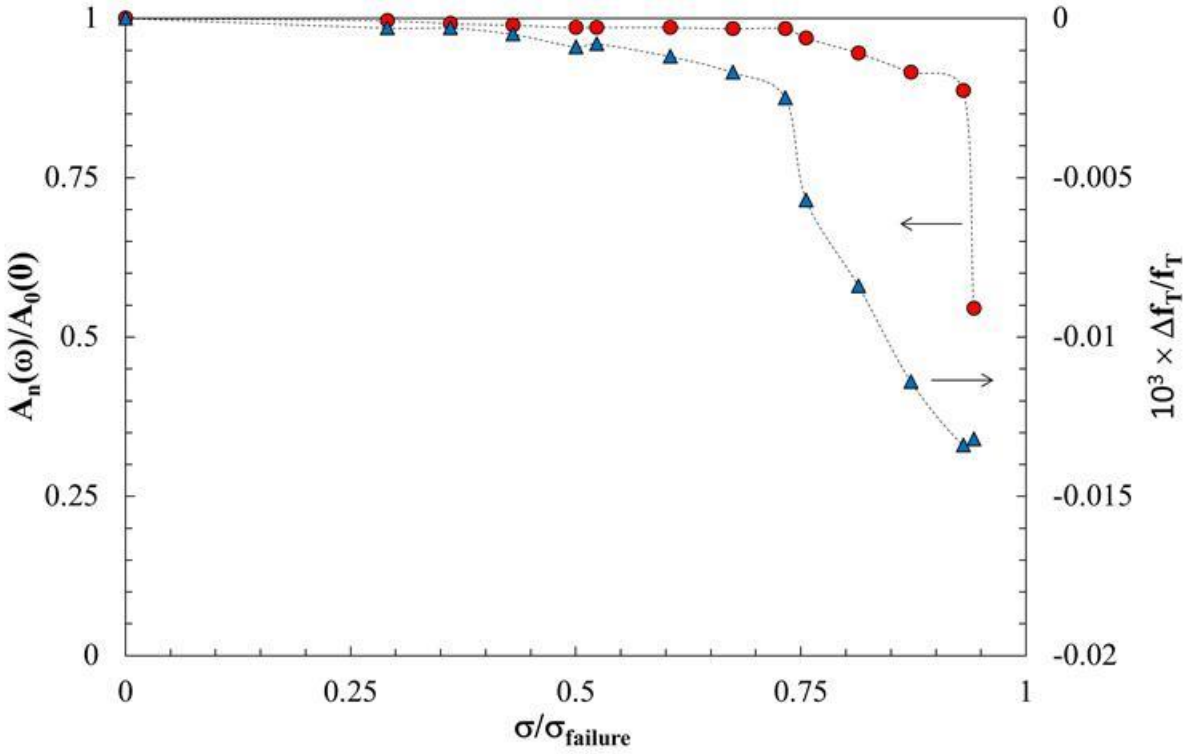

Figure 10. Normalized peak cross-correlation, $A_n(\omega)/A_0(0)$, (circular markers) and normalized change in peak frequency, $\Delta f_T/f_T$, (triangular markers) versus normalized peak-stress, $\sigma/\sigma_{failure}$, for static testing of three lap-shear coupons (Sample 'B4N1', thickness mode, T_1)

Fatigue loading

One single lap-joint sample was dynamically tested by applying a sinusoidal, unidirectional axial load with load ratio R= 0.2. The peak stress on the adhesive during the loading phase had a magnitude of 1.7 *MPa* and the testing frequency was set at 3*Hz*. The sample had a single transducer at the center of a 2.5 *cm* × 2.5 *cm* bond-line that had been intentionally contaminated by graphite powder at manufacturing. The sample was paused and unloaded every 500 cycles and the admittance of the embedded transducer recorded.

Figure 11 shows the results obtained by compiling the data from the fatigue testing up to structural failure at 47,500 cycles. The cross-correlation analysis results shown in Figure 10(b) are based on the transducer's conductance, $G_n(\omega)$, similarly to the analysis carried out for the static tests. Conversely Figure 11(a) shows the cross-correlation carried out using the real part of the impedance, $Re(Z_n)$. In both plots both $A_n(\omega)/A_0(0)$ and $\Delta f_R/f_R$ are relatively stable up until 60% of the sample's life but a definite local minimum for either parameter is not observable in Figure 11(b). When the normalized peak cross-correlation, $B_n(\omega)/B_0(0)$, and the parameter $\Delta f_R/f_R$ are computed using the real part of the impedance, a distinctive local minimum for $\Delta f_R/f_R$, is

observed at about 60% of the fatigue life, whereas $B_n(\omega)/B_0(0)$ shows a local minimum at about 90% of the fatigue life of the sample.

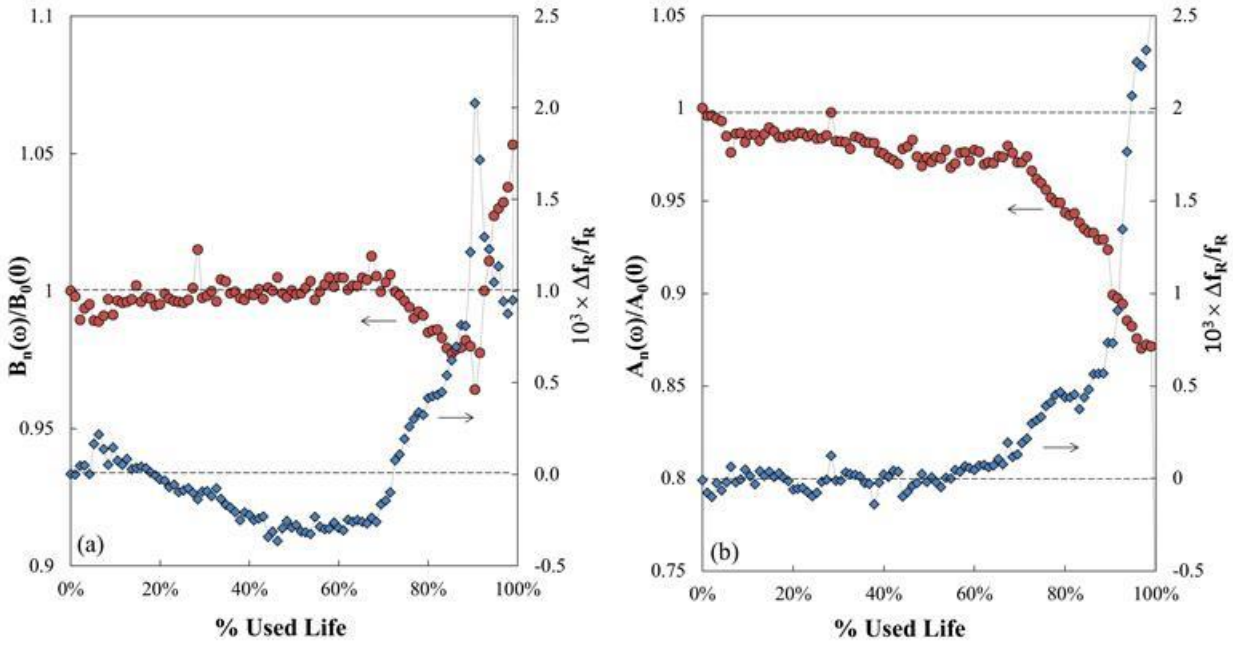

Figure 11. (a) Normalized peak cross-correlation, $B_n(\omega)/B_0(0)$, (circular markers) based on $Re(Z)$ versus percentage of life used, and normalized change in peak frequency, $\Delta f_R/f_R$, versus percentage of life used (diamond markers) from dynamic testing of one lap-joint coupons. (b) Normalized peak cross-correlation, $A_n(\omega)/A_0(0)$, (circular markers) based on $G(\omega)$ versus percentage of life used, and normalized change in peak frequency, $\Delta f_R/f_R$, (diamond markers) versus percentage of life used from dynamic testing of one lap-joint coupons (N_f = 47,500; R = 0.2, f = 3 Hz, σ_{max} = 1.7 MPa).

DISCUSSION

In this section the results from the static and fatigue testing carried out on the shear-lap joints with transducers embedded are discussed. The experimental results are also compared with the findings from the FEM and the analytical solution proposed by Dugnani and Chang[12].

First Radial Resonant Mode

The behavior of the parameters $A_n(\omega)/A_0(0)$ and $\Delta f_R/f_R$ was studied based on the experimental results conducted on various lap-joints with embedded piezoelectric transducers. Figure 6 tracks both $A_n(\omega)/A_0(0)$ and $\Delta f_R/f_R$ versus the normalized peak average stress from the static tests conducted on three exemplary lap-joints not contaminated by the graphite powder. For the data presented, both the parameters $A_n(\omega)/A_0(0)$ and $\Delta f_R/f_R$ display a relatively stable behavior at low stress levels. Nonetheless, the parameter $\Delta f_R/f_R$ shows a distinguishable local minimum before failure in the range $0.8 < \sigma/\sigma_{failure} < 0.9$, whereas the parameter $A_n(\omega)/A_0(0)$ does not always show a local minimum. The exact reasons for the inconsistency in the behavior of $A_n(\omega)/A_0(0)$ is not fully understood but a plausible explanation is that the data was not collected

frequently enough to capture the local minimum for the parameter $A_n(\omega)/A_0(0)$. This explanation is partially supported by the results of the FEM study introduced in the previous section. The FEM results (Figure 5) shows that a local minimum for the parameter $\Delta f_R/f_R$ occurs when the weakened interface covers approximately 76% of the bonded area; nonetheless, for the parameter $A_n(\omega)/A_0(0)$ a minimum occurs as the weakened interface approaches 99% of the bonded area, suggesting that the minimum is likely to occur shortly before failure.

Another possible explanation for not capturing a discernable minimum for the parameter $A_n(\omega)/A_0(0)$ is that the adhesive's loss factor, η_b, is expected to influence the parameter $A_n(\omega)/A_0(0)$ but not $\Delta f_R/f_R$ as suggested by the work of Dugnani and Chang[20]. The dependence of $A_n(\omega)/A_0(0)$ on the adhesive's loss factor, η_b, is expected to be reflected in a relatively unstable signal as external factors such as humidity and temperature influence its behavior. Hence, a local minimum is likely to be more difficult to capture if the transducer's signal is affected by external noise.

Figure 8 summarizes the results of the static tests carried out on contaminated (dark markers) and non-contaminated (light markers) bond-lines. The plot shows on the y-axis the value of the average shear stress corresponding to the local minimum of the function $\Delta f_R/f_R$ and on the x-axis the stress at failure, $\sigma_{failure}$, for the same sample. The figure presents both the case for transducers placed at the center of the bond-line (i.e., at $L_b/2$), and the case for the transducer near the edge of the bond-line (i.e., at at $L_b/8$). For the case where the transducers were embedded at $L_b/2$, the function $\Delta f_R/f_R$ reaches a minimum at $\sigma \cong 0.84 \cdot \sigma_{failure}$, whereas for the case where the transducer was place at $L_b/8$, a local minimum is reached at approximately $\sigma \cong 0.6 \cdot \sigma_{failure}$. Comparatively by using the damage index method with a threshold at 6% as proposed by Zhuang et al.[18] damage in the bond-line could be detected at a significantly later stage in the life of the component (12% to 22% higher damage). In particular, Zhuang et al.[18] reported for the case where the transducers were embedded at $L_b/2$, failure could be detected at $\sigma = 0.96 \cdot \sigma_{failure}$, whereas for the case where the transducer was place at $L_b/8$, failure is detected at $\sigma = 0.78 \cdot \sigma_{failure}$. This behavior is consistent with the damage propagation scenario proposed and described in the FEM section. It is expected that for a transducer located closer to the edge of the bond-line, the interface's degradation reaches the transducer earlier in the life of the component compared to the case where the transducer is located at the center of the bond-line. This behavior also suggests that the strategic placement of transducers in the bond-line might be exploited to yield warnings at various stages in the life of the structure.

Although the placement of the transducers near the edge of the adhesive might initially appear as a better opportunity for detecting early failures, it should also be noted that transducers located near the edge of the adhesive are also exposed to higher shear-stresses during the life of the part[31]. Furthermore, it is possible that the bond-line damage in some cases might initiate asymmetrically on one side of the bond-line rather than on both sides. It follows that twice as many transducers are necessary for the case where the transducers are embedded near the edges compared to the case where the transducers are embedded at the center of the bond-line. Finally, transducers located near the edge of the bond-line might introduce stress concentration and have

a negative impact on the life of the component whereas transducers located at the center of the bond-line will likely not induced any significant stress concentration under normal loading conditions[31].

Thickness Resonant Mode

Similarly to the first radial mode (R_1), the analysis of the EMI signal for the first thickness mode (T_1) shows significant changes to both the parameters $A_n(\omega)/A_0(0)$ and $\Delta f_T/f_T$, as the loading approaches structural failure (Figure 10). Regardless of the apparent similarity in the results, some fundamental differences exist between the outcome of the analysis on R_1 and T_1. First, as a result of the dominant longitudinal motion of the transducer, SV-waves traveling along the length of the bond-line are generated at resonance[20]. Conversely, for transducers resonated in the thickness mode, the transducer's displacement occurs mostly in the thickness direction and P-waves traveling in a direction orthogonal to the face of the plates are predominantly generated at resonance. In the analysis of the response of the transducer resonated in the thickness mode, a substantial complication is introduced by the interaction of the acoustic waves with the aluminum plates. In this case, the P-waves (and to a lesser degree, the SV-waves) generated by the transducer are reflected by the higher acoustic impedance plates and travel back towards the actuator[40]. The reflected pressure waves generate an interference patter with the incoming wave which affects the response of the transducer[41]. In fact, when the reflected waves are in phase with the emitted waves the adhesive "appears" stiffer and the EMI signal decreases. A similar type of behavior induced by the presence of highly reflective boundaries near the emitting transducer has been described by Alers et al.[42], and by Weise et al.[11]. For a highly reflecting surface, this occurs when the thickness of the adhesive located directly above the transducer, t_{b0}, has a value near the one described by Equation 6:

$$t_{b0} = \frac{(n+1)\lambda_i}{2} \qquad n \in 0,1,2,... \tag{6}$$

where λ_i, is the wavelengths corresponding to the relevant acoustic wave considered. Equation 6 can also be expressed in terms of the frequency, f_n, for which an "antinode" is located at the surface of the emitting transducer:

$$f_{n,i} = \frac{c_i}{2t_{b0} \cdot n} \tag{7}$$

The term c_i in Equation 7 refers to both the speed of sound of the SV-wave (i= 1) and of the P-wave (i= 2).

Some approximate calculations are carried out and presented to estimate the antinode frequencies for the specific cases analyzed. For the adhesive material used (Hysol EA 9696) the speed of the pressure wave is calculated based on the adhesive's mechanical properties as $c_2 \cong$ 1430 *m/sec*, and $c_2/c_1 \cong$ 2.1. Assuming the thickness of the adhesive film $2t_{b0}$= 0.1 *mm*, strong interference in the frequency range of the thickness mode are expected to occur at $f_{5,1}$= 8.3 *MHz*, (SV-waves antinode), and $f_{2,2}$= 7.1 *MHz* (P-waves antinode). Figure 12(a) shows schematically the expected conductance, $G(\omega)$, at resonance for a transducer embedded in an infinitely thick

adhesive. Figure 12(b) shows the signal gap due to the interference patter between the incoming and the reflected waves. Finally, Figure 12(c) depicts schematically the expected behavior of the conductance, $G(\omega)$, as a result of the interaction with the aluminum plates. Figure 12 on the left-hand side shows the conductance, $G(\omega)$, for frequencies corresponding to the transducer's thickness resonance mode. In this case, the conductance is plotted versus the transducer's excitation frequency for the 23 loading cycles prior to the sample's structural failure. Each signal was obtained as the load was incrementally increased in steps of 0.3 *MPa* to a final value of 6 *MPa*. Both the resonant frequency and the amplitude of conductance appear to be affected by the cycling of the transducer yet the frequency gaps at 8.2 *MHz* and 7.2 *MHz* remain unchanged (Figure 12). Such behavior can be explained by the fact that although the boundaries between the adhesive and the adherend are affected by the testing, both the speed of sound and the thickness of the adhesive film are not. This behavior is consistent with the interference pattern described by Equations 6 and 7, and with progressive damage being introduced at the adherend/adhesive interface during mechanical testing. Due to the complicated interaction with the highly acoustically reflective aluminum plates, the analysis of $B_n(\omega)/B_0(0)$ and $\Delta f_T/f_T$ becomes extremely difficult and hence in this study it is not used as a valuable indicator of the bond-line degradation.

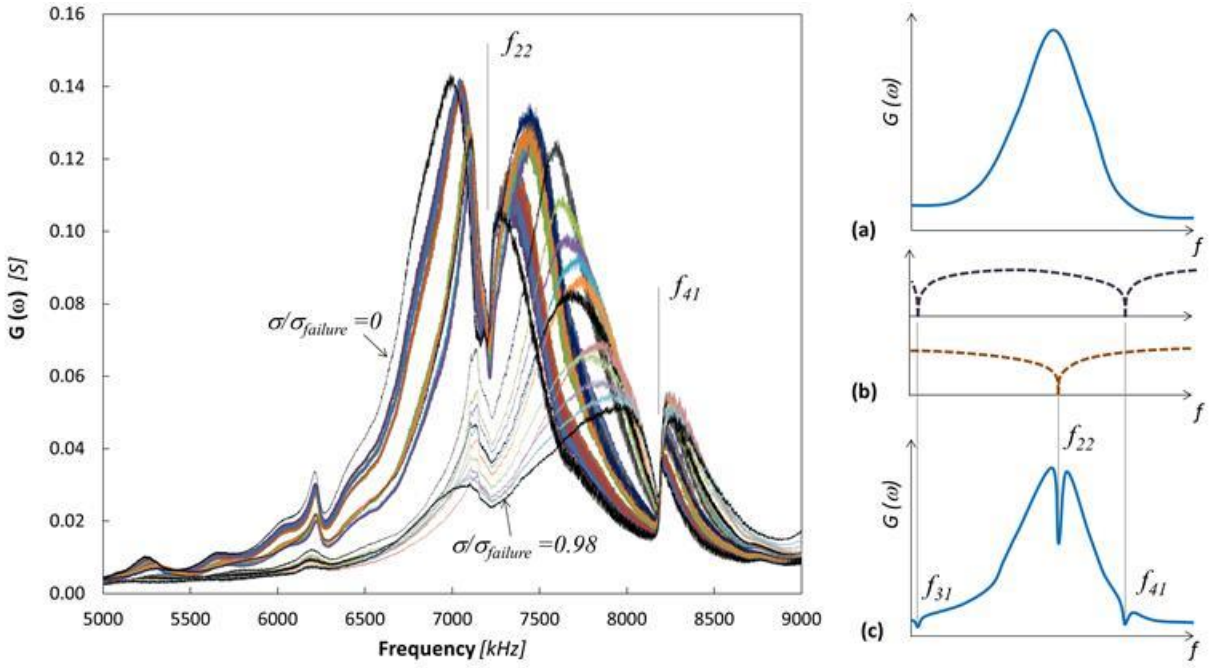

Figure 12. Conductance, $G(\omega)$, versus the transducer's excitation frequency for various normalized peak-stress, $\sigma/\sigma_{failure}$. A gap in the magnitude is clearly visible for all traces at identical frequency range as a result of the frequency dependent transmission in the aluminum plates (Sample 'B4N1'; $\sigma_{failure} = 6$ *MPa*).

Fatigue Test

Fatigue testing was carried out on a single lap-joint coupon contaminated at the adherend's interface by graphite powder. The lap-joint used in the fatigue test had a piezoelectric

transducer embedded in the adhesive which was used to collect the admittance signal at frequencies near the first radial mode. Figure 11 shows some of the results compiled from the analysis of the fatigue data up to 47,500 cycles, when structural failure occurred. Figure 11 shows $\Delta f_R/f_R$ both as computed based on the conductance, $G(\omega)$, and also computed based the real part of the impedance, $Re(Z)$. In the static test case, the parameter $\Delta f_R/f_R$ as computed using the conductance signal was found to display a local minimum for a shear load corresponding to 84% of the structural failure. Interestingly, for the fatigue test, the computed parameter $\Delta f_R/f_R$ displays similar behavior to the static case only when the real part of the impedance rather than the conductance was used in the analysis. The reason for this behavior is not fully understood and might be related to either a fundamentally different damage propagation mode compared to the model considered, or possibly due to the excessive contamination of the bond-line for the case tested. Clearly were the initial degradation already at an advanced stage a local minimum should not be observable for neither $\Delta f_R/f_R$ nor $A_n(\omega)/A_0(\omega)$.

CONCLUSION AND FUTURE WORK

In this paper we presented a study on lap-joint integrity monitoring using the EMI signal from piezoelectric transducers embedded in the adhesive bond-line. The method hinged on monitoring changes over time of key parameters obtained from the transducers' EMI signature and using the minimum of such parameters as damage indicators. The proposed technique was able to predict damage in the bond-line at significantly earlier stages during the life of the component. In particular damage in the parts was predicted 12% to 22% earlier compared to the analysis on the same parts using the damage index method with a threshold at 6% as proposed by Zhuang et al.[18]. Although the proposed method appeared to be better than Zhuang et al.[18], nonetheless the proposed method should be used concurrently with the damage index-based method. In fact, although the proposed minimum-detection method is expected to predict damage at earlier stages in the life of the component, it is possible that if a significant overload were to occur during the service life of the structure, the minimum for the monitored parameters might not be recorded, whereas a spike in the damage index would always be observable.

In the work presented, the influence of weaker bond-lines on the EMI signature was also analyzed by means of the analytical solution proposed by Dugnani and Chang[20] as well as by a FEM simulation. The results from the mechanical testing and from the numerical analysis indicated that the method proposed is very effective in predicting the failure of the bond-line for both the standard and the weak bond-lines. Specifically, when the transducer was embedded at the center of the bond-line, local damage to the bond-line was consistently detected at approximately 84% of the maximum failure load for statically loaded structures. For the case of a transducer embedded near the edge of the bond-line the failure of the lap-joint was detected as early as at 60% of the maximum load. Preliminary fatigue tests also showed that significant changes in the EMI signals were apparent starting at 60% of the life of the bond-line.

Future work should include additional testing to confirm the validity of the proposed method under various testing conditions and failure modes. A detail study on the placement and size of the piezoelectric transducers is strongly recommended since different locations of the transducers would likely result in warnings at different stages in the life of the adhesive. The influence of the transducer's geometry such as shape and thickness should also be considered. In particular in the next stage of testing, minimally invasive piezoelectric micro-sensors (such as 20-30 μm-thick transducers currently being developed at Stanford University by screen-printing technique) should be utilized.

A possible limitation of the study presented was to consider the EMI response for the first extensional mode but higher extensional modes might be considered in the future to potentially improve the prediction of the structural failure. Further work is also recommended to include different damage propagation scenarios and/or concurrently carry out conventional ultrasonic scans of the structure to establish a correlation between current NDT techniques and the proposed SHM method. The current study focused on debonding at the adhesive/adherend interface but clearly the response of the transducer when cohesive failure of the adhesive film occurs is also of great interest.

Finally, the effect of changing the voltage excitation of the transducer should be investigated. In the present work a voltage of 0.2 V was used in all experiments. Yet, since weaker bond-lines such as 'kissing bonds' are expected to react differently depending on the intensity of the wave interacting with the interface, the effect of the voltage on the signal could provide valuable information to assess the presence of weaker bond-lines. This effect should be study particularly for transducers resonated in the thickness mode since the interaction between the reflective plate and the transducer allows the generation of high-energy acoustic waves.

ACKNOLEGMENTS

The authors would like to extend their gratitude to Stanford University's SACL members Cheng Liu for preparing the samples and helping conducting the experimental tests, and Raphael Nardari for his help and technical support with the FE analysis.

References

1. Kouhei T, Soejima H, Nakajima M, Yoji O, and Nobuo T. Bond Line Monitoring Technology for Aircraft CFRP Structure Using Lamb Wave. *Proceedings of 10th International Workshop on Structural Health Monitoring* (2015).
2. Preisler A, Sadeghi Z, Adomeit A, Schröder, K-U. Damage Assessment in Adhesively Bonded Structures by Using SmartSHM. *Proceedings of 10. Proceedings of 10th International Workshop on Structural Health Monitoring* (2015).
3. Poveromo S, Malcolm D, Earthman J. Percussion Diagnostics for Evaluating the Strength of Bonds between Composite Laminates. *Proceedings of 10th International Workshop on Structural Health Monitoring* (2015).

4. Malinowski P, Wandowski T, Ostachowicz W. Study on Adhesive Bonds Influence on EMI Signatures. *Proceedings of 10th International Workshop on Structural Health Monitoring* (2015).
5. Malinowski P, Wandowski T, Ostachowicz W. The use of electromechanical impedance conductance signatures for detection of weak adhesive bonds of carbon fiber–reinforced polymer. *Structural Health Monitoring* 2015; DOI: 10.1177/1475921715586625.
6. Malinowski P, Tserpes KI, Wandowski T, Skarbek L, Ostachowicz W. Composite bonds assessment using EMI technique. *Structural Health Monitoring* 2013; 1–2: 2407–2414.
7. Gulizzi V, Rizzo P, Milazzo A. Electromechanical Impedance Method for the Health Monitoring of Bonded Joints: Numerical Modeling and Experimental Validation. *SDHM: Structural Durability & Health Monitoring* 2014; 10.1: 19-54.
8. Jones R, Galea S. Health monitoring of composite repairs and joints using optical fibers. *Composite Structures* 2002; 58(3): 397-403.
9. Murayama H, Kageyama K, Uzawa K., Ohara K. and Igawa H. Strain monitoring of a single-lap joint with embedded fiber-optic distributed sensors. *Structural Health Monitoring* 2012; 11(3): 325-344.
10. Smith RA, Weise VL and Dalton RP. The Potential for Advanced Ultrasonic Detection of Weak Adhesion. QinetiQ Ltd 2003; 1-5.
11. Weise VL, Tucker JR, Bruce DA, Smith RA. An initial investigation into the relationship between the material properties of adhesive joints and their ultrasonic spectral properties. *Review of Progress in Quantitative Non-Destructive Evaluation* 2001; 20. Vol. 557(1); AIP Publishing.
12. Roach D, Rackow K and Duvall R. Innovative use of adhesive interface characteristics to nondestructively quantify the strength of bonded joints. *10th European Conference on Non-Destructive Testing* (2010).
13. Nagy PB. Ultrasonic detection of kissing bonds at adhesive interfaces. *Journal of Adhesion Science and Technology* 1991; 5(8): 619-630.
14. Munns IJ, Georgiou GA. Non-destructive testing methods for adhesively bonded joint inspection: a review. *Insight* 1995; 37(12): 941-952.
15. Clark AV and Hart SD. Measurement of Ultrasound Reflected from Liquid Layers of Submicron Thickness. *Materials Evaluation* 1982; 7: 866-873.
16. Cheng J, Taheri F. A smart single-lap adhesive joint integrated with partially distributed piezoelectric patches. *International journal of solids and structures* 2006; 43(5): 1079-1092.
17. Di Scalea FL, Rizzo P and Marzani A. Propagation of ultrasonic guided waves in lap-shear adhesive joints: Case of incident a0 Lamb wave. *The Journal of the Acoustical Society of America* 2004; 115(1): 146-156.
18. Zhuang Y, Kopsaftopoulos F and Chang FK. Bondline Integrity Monitoring of Adhesively Bonded Structures via Electromechanical Impedance Based Approach. *Proceedings of 10th International Workshop on Structural Health Monitoring* (2015).
19. Tucker JR and Birmingham AL. Ultrasonic Spectroscopy using a Rapid Sweep Technique. *WCNDT* 2004; 9(11).
20. Dugnani R, Chang F-K. Analytical Model of Lap-joint Adhesive with Embedded Piezoelectric Transducer for Weak Bond Detection. *Journal of Intelligent Material Systems and Structures* 2015 [in print].
21. Liang C, Sun FP and Rogers CA. Coupled electro-mechanical analysis of adaptive material systems—determination of the transducer power consumption and system energy transfer. *Journal of Intelligent Material Systems and Structures* 1994; 5(1): 12-20.

22. Pilarski A, Rose JL. Ultrasonic oblique incidence for improved sensitivity in interface weakness determination. *NDT International* 1998; 21(4): 241-246.
23. Lavrentyev AI, Rokhlin SI. Models for ultrasonic characterization of environmental degradation of interfaces in adhesive joints. *Journal of applied physics* 1994; 76(8): 4643-4650.
24. Rokhlin SI, Xie B and Baltazar A. Quantitative ultrasonic characterization of environmental degradation of adhesive bonds. *Journal of adhesion science and technology* 2004; 18(3): 327-359.
25. Wang N, Lobkis OI, Rokhlin SI, Cantrell JH. Ultrasonic characterization of interfaces in composite bonds. *Review of the Progress in Quantitative Nondestructive Eval*. 2011; 30: 1079-1086.
26. Moidu AK, Sinclair AN, Spelt JK. Nondestructive characterization of adhesive joint durability using ultrasonic reflection measurements. *Research in nondestructive evaluation* 1999; 11(2): 81-95.
27. Tattersall HG. The ultrasonic pulse-echo technique as applied to adhesion testing. *Journal of Physics D: Applied Physics* 1973: 6(7): 819.
28. Baltazar A, Wang L, Xie B and Rokhlin SI. Inverse ultrasonic determination of imperfect interfaces and bulk properties of a layer between two solids. *The Journal of the Acoustical Society of America* 2003; 114(3): 1424-1434.
29. ASTM D 1002–10 Standard Test Method for Apparent Shear Strength of Single-Lap-Joint Adhesively Bonded Metal Specimens by Tension Loading (Metal-to-Metal). ASTM international, 2010.
30. Henkel AG & Company website. http://www.henkelna.com/, March 2015.
31. Ha S, Lonkar K, Mittal A and Chang FK. Adhesive layer effects on PZT-induced lamb waves at elevated temperatures. *Structural Health Monitoring* 2010; 9(3): 247-256.
32. Mc Hugh J, Döring J, Stark W and Erhard A. Characterization of epoxy materials used in the development of ultrasonic arrays. *Proceedings, 16th World Conference on NDT* 2004.
33. APC International website. https://www.americanpiezo.com/, March 2015.
34. SinePhase website. http://www.sinephase.com/, March 2015.
35. ASTM D3136-99 Standard Test Method for Fatigue Properties of Adhesives in Shear by Tension Loading (Metal/Metal). ASTM International, 1999.
36. Dugnani R. Monitoring Adhesive Integrity of PZT Transducer by Electromechanical Impedance Technique. *J. of Intelligent Material Systems and Structures* 2013. doi: 10.1177/1045389X13486714.
37. Giurgiutiu V and Rogers CA. Modeling of the electro-mechanical (E/M) impedance response of a damaged composite beam. *Adaptive Struct. Mater. Syst* 1999; 87: 39-46.
38. Postema M. Fundamentals of medical ultrasonics. CRC Press, 2011.
39. Da Silva LF, das Neves PJ, Adams RD and Spelt JK. Analytical models of adhesively bonded joints—Part I: Literature survey. *International Journal of Adhesion and Adhesives* 2009; 29(3): 319-330.
40. Guyott CCH, Cawley P and Adams RD. The non-destructive testing of adhesively bonded structure: a review. *The Journal of Adhesion* 1986; 20(2): 129-159.
41. Kinsler LE, Frey AR, Coppens AB, Sanders JV. Fundamentals of acoustics. 4th Edition, ISBN 0-471-84789-5. Wiley-VCH, December 1999.

42. Alers GA, Elsley RK and Flynn PL. Measurement of Strength of Adhesive Bonds. *Proceedings of the ARPA/AFML Review of Progress in Quantitative NDE* 1978.